3640 *Biochemistry* **2010,** *49,* 3640–3647
DOI: 10.1021/bi100328j

BIOCHEMISTRY
including biophysical chemistry & molecular biology
Article

Evidence for a Bicarbonate "Escort" Site in *Haemophilus influenzae* β-Carbonic Anhydrase[†,‡]

Roger S. Rowlett,* Katherine M. Hoffmann, Hannah Failing, Margaret M. Mysliwiec, and Dejan Samardzic

Department of Chemistry, Colgate University, 13 Oak Drive, Hamilton, New York 13346

Received March 4, 2010; Revised Manuscript Received March 31, 2010

ABSTRACT: The *Haemophilus influenzae* β-carbonic anhydrase (HICA) allosteric site variants V47A and G41A were overexpressed and purified to homogeneity. These variants have k_{cat}/K_m values similar to that of the wild-type enzyme and exhibit a similar dramatic decrease in catalytic activity at pH < 8.0. However, both HICA-G41A and -V47A were serendipitously found to bind sulfate ion or bicarbonate ion near pairs of Glu50 and Arg64 residues located on the dimerization interface. In the case of HICA-V47A, bicarbonate ions simultaneously bind to both the dimerization interface and the allosteric sites. For HICA-G41A, two of 12 chains in the asymmetric unit bind bicarbonate ion exclusively at the dimerization interface, while the remaining 10 chains bind bicarbonate ion exclusively at the allosteric site. We propose that the new anion binding site along the dimerization interface of HICA is an "escort" site that represents an intermediate along the ingress and egress route of bicarbonate ion to and from the allosteric binding site, respectively. The structural evidence for sulfate binding at the escort site suggests that the mechanism of sulfate activation of HICA is the result of sulfate ion competing for bicarbonate at the escort site, preventing passage of bicarbonate from the bulk solution to its allosteric site.

Carbonic anhydrases (carbonate hydrolyase, EC 4.2.1.1, CA)[1] are metalloenzymes that catalyze the interconversion of CO_2 and bicarbonate:

$$CO_2 + H_2O \leftrightarrows HCO_3^- + H^+ \quad (1)$$

The β-CAs make up one of five convergently evolved classes of CA and are widespread in eubacteria and plants. All β-CAs that have been characterized to date are zinc metalloenzymes. *Haemophilus influenzae* carbonic anhydrase (HICA) is a "type II" member of the β-carbonic anhydrase family (*1*). Type II β-CAs are able to adopt a structure in which the catalytically essential zinc-bound water molecule can be displaced by an active site Asp residue. In addition, type II β-CAs have a characteristic triad of noncatalytic residues (Trp39, Arg64, and Tyr181 in HICA) ~8 Å from the active site zinc ion that can bind bicarbonate ion. For HICA and ECCA, kinetic and structural evidence strongly suggests that this noncatalytic bicarbonate ion is a negative allosteric effector that stabilizes an inactive, T-state conformation of the enzyme, where Asp44 displaces the catalytically essential zinc-bound water (*2*). The X-ray crystallographic structures of type I (nonallosteric) β-CAs and the D44N variant of HICA suggest that type II β-CAs can also adopt an active, R-state conformation in which Asp44 pairs with Arg46, allowing the coordination of the catalytically essential water molecule to the active site zinc ion (*3*). The noncatalytic bicarbonate ion is believed to stabilize the inactive T state (Scheme 1), and this hypothesis is borne out by the W39F variant of HICA in which bicarbonate ion is significantly less effective in inhibiting the enzyme (*3*).

A key player in the allosteric (T → R) transition of HICA in Scheme 1 is Val47: the steric bulk of this side chain is hypothesized to displace bicarbonate from the allosteric binding site in the R state and thus provides the necessary steric coupling mechanism between the bicarbonate binding and the adopted allosteric state. In addition, examination of X-ray crystallographic structures of type I and type II β-CA reveals that type I β-CAs all have a slightly more bulky Ala41 residue rather than the smaller Gly41 in type II β-CAs. Examination of type II β-CA structures with Gly41 altered to Ala suggests that this structural change may preclude bicarbonate binding to the allosteric site (*1*). To investigate the roles of these residues, we kinetically and structurally characterized the G41A and V47A variants of HICA.

Surprisingly, we find that these variants have little impact on the catalytic function of HICA. However, we have serendipitously discovered that these variants are able to bind bicarbonate ion in an intermediate binding site that apparently defines the entry and exit pathway of bicarbonate to and from the allosteric site, respectively. These results suggest that the mechanism of allosteric inhibition of HICA and the selectivity of the allosteric binding site are more complex than previously recognized.

EXPERIMENTAL PROCEDURES

Expression and Purification of Wild-Type and Recombinant Enzymes. Wild-type HICA was prepared as previously described (*2*). Site-directed mutations of the gene encoding

[†]This work was supported in part by a grant (to R.S.R.) from the National Science Foundation (MCB-0741396).

[‡]Coordinates and structure factors have been deposited in the Protein Data Bank as entries 3E2X, 3E31, 3E3F, 3E3G, and 3E3I.

*To whom correspondence should be addressed. E-mail: rrowlett@colgate.edu. Phone: (315) 228-7245. Fax: (315) 228-7935.

[1]Abbreviations: CA, carbonic anhydrase; HICA, *H. influenzae* β-carbonic anhydrase; ECCA, *Escherichia coli* β-carbonic anhydrase; ICP-OES, inductively coupled plasma optical emission spectroscopy; EDTA, *N*,*N*,*N*′,*N*′-ethylenediaminetetraacetic acid; PCR, polymerase chain reaction; PEG-400, polyethylene glycol 400; HEPES, 4-(2-hydroxyethyl)piperazineethanesulfonic acid; PDB, Protein Data Bank; rmsd, root-mean-square deviation.

 Published on Web 04/01/2010

Scheme 1: Structural Schematic of Key Active Site and Noncatalytic Bicarbonate Binding Site Interactions in the Hypothesized Active (R-state) and Inactive (T-state) Conformations of HICA (*2*)

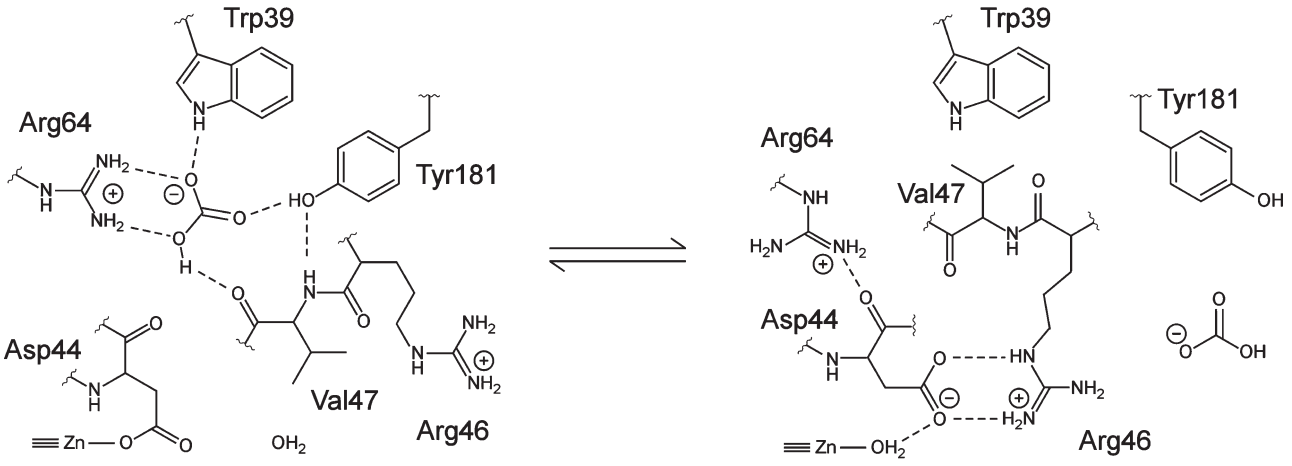

HICA were constructed using megaprimer PCR (*4*) with *Vent* (New England Biolabs) or *Pfu* turbo (Stratagene) polymerase and commercial oligonucleotides (Integrated DNA Techonolgies). For variant V47A, a mutated oligonucleotide[2] 5′-TTCAGCAGGC**CGC**ACGGCTATC-3′ was paired with the 5′ oligonucleotide primer PHI1X (5′-TGCCCATGGATAAAATTAAACAACTCTTT-3′) in the first PCR to give a 129 bp product. This PCR product was used as a megaprimer in a second PCR with the 3′ oligonucleotide primer PHI2X (5′-TGCCTGCAGTTATTATGTATTTTCAAGATG-3′) to create the final mutated HICA gene. The final PCR product was digested with *Nco*I and *Pst*I (Promega) and ligated (Quick Ligase, New England Biolabs) into the pTrc99a vector digested with the same enzymes. Variant G41A was constructed similarly using the mutated oligonucleotide 5′-ATCAGAGCAA**AGC**AATCCAAAG-3′. All expression plasmids were subjected to DNA sequencing (PE Biosystems ABI 310, BigDye 3.0 chemistry) of the entire HICA gene to verify introduction of the correct mutation.

Expression, purification, storage, and quantification of variant HICA proteins were exactly as described for the wild-type protein (*2*). Briefly, crude homogenates of the overexpressed protein were purified to homogeneity by ion exchange (Q-Sepharose FF), hydrophobic interaction (butylsepharose FF), and gel exclusion chromatography (Superdex 200) using an AKTA FPLC system (GE Healthcare) and quantified by ICP-OES (Perkin-Elmer Optima SC 3000) for zinc at 213.856 nm.

Steady-State Kinetic Methods. We prepared saturated solutions of CO_2 by bubbling CO_2 gas into water in a vessel maintained at 25.0 ± 0.1 °C and dilutions in the absence of air by coupling two gastight syringes as described by Khalifah (*5*). CO_2 concentrations were calculated on the basis of a 33.8 mM saturated solution at 25 °C (*6*).

All steady-state kinetic measurements were taken at 25 °C using a Hi-Tech SF-61DX2 stopped-flow spectrophotometer. Initial rates of CO_2 hydration were measured using the changing pH-indicator method described previously (*5*, *7*, *8*). All stopped-flow kinetic studies were conducted in the presence of 250 mM Na_2SO_4, which was required for maximum enzyme stability and activity in dilute solution (*2*). Values of k_{cat} and K_m were determined by nonlinear least-squares fits to v/[E] versus [CO_2] data using Origin 7.0 (Microcal). For all kinetics measurements reported here, the substrate dependence of CO_2 hydration rates appeared to follow Michaelis−Menten kinetics. The kinetic constants k_{cat} and k_{cat}/K_m are reported here on a per subunit basis.

Crystallographic Methods. Starlike clusters of orthorhombic plates of HICA-V47A appeared after 3 months in 1.7 M ammonium sulfate, 4% PEG-400, 0.10 M HEPES (pH 7.50), and 6 mg/mL protein at 4 °C using hanging drop vapor diffusion. Crystals were soaked in artificial mother liquor and 30% glucose for 30−60 s prior to being flash-cooled in liquid nitrogen. Data collection for PDB entry 3E2X was conducted at beamline F2 of CHESS at a wavelength of 0.98 Å detector using 0.5° oscillations at a temperature of 100 K.

Tetragonal crystals of HICA-V47A were grown in 2−3 days in 0.7 M sodium potassium tartrate, 0.10 M HEPES (pH 7.50), and 12 mg/mL protein at 22 °C. Crystals were soaked for 1−2 min in artificial mother liquor with either 30% glucose (PDB entry 3E31) or 30% glucose and 100 mM $NaHCO_3$ (PDB entry 3E3F) before being flash-cooled in liquid nitrogen. Data collection was conducted at beamline F2 of CHESS at a wavelength of 0.98 Å detector using 0.5° oscillations at a temperature of 100 K.

Monoclinic crystals of HICA-G41A were grown in 2−3 days in 1.8 M ammonium sulfate, 4% PEG-400, 0.10 M HEPES (pH 7.50), and 12 mg/mL protein at 22 °C. Crystals were soaked for 1−2 min in artificial mother liquor with either 30% glucose (PDB entry 3E3G) or 30% glucose and 100 mM $NaHCO_3$ (PDB entry 3E3I) before being flash-cooled in liquid nitrogen. Data collection was conducted at beamline F2 of CHESS at a wavelength of 0.98 Å detector using 0.5° oscillations at a temperature of 100 K.

Data were processed using MOSFLM (*9*) and SCALA (*10*), and an initial molecular replacement solution as obtained by using a search model using a single dimer (HICA-V47A) or three tetramers (HICA-G41A) of wild-type HICA (PDB entry 2A8D) in Phaser (*11*). The initial solution was subjected to multiple rounds of refinement using Refmac5 (*12*) and model building in Coot (*13*). Final refinement used TLS (*14*) with one TLS group per protein chain.

Data collection and refinement statistics are listed in Table 1.

[2]Mutation sites of oligonucleotides are shown in bold; restriction endonuclease sites for cloning are underlined.

Table 1: Data Collection and Refinement Statistics for HICA Variants[a]

	G41A (PDB entry 3E3G)	G41A with 100 mM HCO_3^- (PDB entry 3E3I)	V47A (PDB entry 3E2X)	V47A (PDB entry 3E31)	V47A with 100 mM HCO_3^- (PDB entry 3E3F)
Data Collection					
source	CHESS beamline F2	CHESS beamline F2	CHESS beamline F2	CHESS beamline F2	CHESS beamline F2
wavelength (Å)	0.97	0.98	0.97	0.97	0.98
space group	*C*2	*C*2	$I2_12_12_1$	$P4_12_12$	$P4_12_12$
cell parameters	231.9 Å, 145.2 Å, 53.0 Å, 90°, 93.8°, 90°	229.6 Å, 144.4 Å, 104.9 Å, 90°, 94.4°, 90°	48.1 Å, 133.3 Å, 143.9 Å, 90°, 90°, 90°	82.3 Å, 82.3 Å, 188.8 Å, 90°, 90°, 90°	83.9 Å, 83.9 Å, 184.9 Å, 90°, 90°, 90°
resolution (Å)	39.4−2.30 (2.36−2.30)	29.8−2.00 (2.05−2.00)	34.0−2.55 (2.62−2.55)	37.7−2.95 (3.11−2.95)	28.9−2.30 (2.42−2.30)
no. of unique reflections	79059	205440	14811	14391	30001
redundancy	6.9 (4.6)	4.8 (3.1)	4.0 (3.2)	16.8 (5.8)	8.2 (4.0)
completeness	98.1 (88.2)	89.6 (55.6)	95.7 (82.0)	99.9 (100)	99.2 (94.6)
R_{sym} (%)	0.088 (0.516)	0.055 (0.475)	0.094 (0.482)	0.082 (0.493)	0.066 (0.367)
$\langle I\rangle/\langle\sigma I\rangle$[b]	19.1 (2.0)	19.1 (1.9)	13.8 (1.6)	34.2 (5.8)	22.6 (2.1)
Refinement					
no. of reflections in the test set	3804	10347	743	718	1523
R_{work} (%)	0.197	0.201	0.211	0.197	0.193
R_{free} (%)	0.234	0.236	0.283	0.247	0.230
no. of atoms					
protein	9959	20350	2920	2887	2894
ligand	85	109	25	0	25
ion	6	12	2	2	2
solvent	133	604	0	16	84
rmsd from ideal[c]					
bond distances (Å)	0.011	0.011	0.013	0.016	0.017
bond angles (deg)	1.2	1.2	1.4	1.6	1.6
Ramachandran plot outliers (%)[d]	2.8	2.4	7.1	5.8	1.9

[a]Values in parentheses represent data for the highest-resolution shell. [b]Reported as $\langle\langle I\rangle/\sigma\langle I\rangle\rangle$ in SCALA or SCALEPACK. [c]Ideal values from ref *20*. [d]Calculated using a strict boundary Ramachandran plot (*13*).

RESULTS

Overexpression and Purification of HICA Variants V47A and G41A. HICA variants V47A and G41A were overexpressed at levels of ≈15% of total protein in *Escherichia coli* and were purified to homogeneity using previously established methods for the wild-type enzyme (*2*). Elution volumes of both HICA-G41A and -V47A on a calibrated gel exclusion column (Superdex-200, Amersham) during the final purification step indicated an apparent molecular mass of ≈100 kDa. This suggests that these variants have the same homotetrameric quaternary structure as the wild-type enzyme.

Sulfate Dependence of HICA Activity. Wild-type HICA requires the presence of sulfate ion in vitro for maximal activity (*2*). Unlike α-CA, which is weakly but significantly inhibited by sulfate ion at near molar concentrations (*15*), HICA is significantly activated by concentrations of sulfate ion up to 400 mM (Figure 1). At higher sulfate concentrations, HICA activity decreases. Like wild-type HICA, variants V47A and G41A have no detectable CO_2 hydration activity in the absence of sulfate ion.

Activity of HICA-V47A and -G41A. Values of k_{cat}/K_m for both HICA-V47A and HICA-G41A have catalytic activity and pH−rate variation similar to those of wild-type HICA. At high pH, the k_{cat} values for HICA-V47A are similar to those of the wild type, but the k_{cat} of HICA-G41A is significantly lower. At pH < 8.0, the catalytic activity of all HICA variants as measured by k_{cat} or k_{cat}/K_m dramatically decreases (Table 2).

Structures of HICA-V47A and -G41A. The overall secondary and tertiary structures of the V47A and G41A variants of HICA are nearly identical to that of the wild-type enzyme. The asymmetric unit of the V47A variants in either the orthorhombic or tetragonal crystal forms is composed of a fundamental dimer of HICA representing the probable simplest functional allosteric unit of the enzyme (*2*). The asymmetric unit of the uncomplexed G41A variant is C2 with dimensions nearly identical to those of the wild-type enzyme (*2*). However, crystals of G41A soaked in 100 mM bicarbonate ion form "double-size" C2 unit cells in which the *c*-axis is approximately twice as long. The apparent doubling in size of the unit cell appears to be the result of the

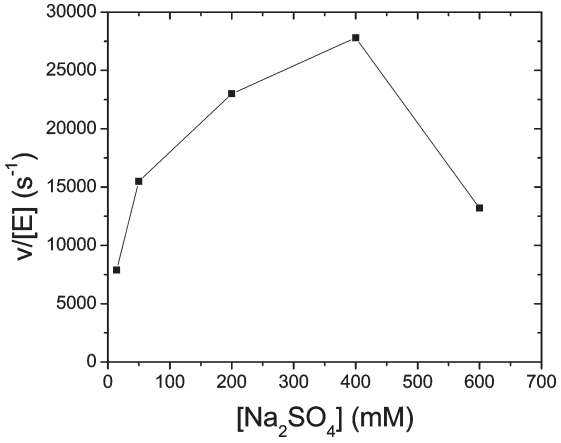

FIGURE 1: Sulfate dependence of the CO_2 hydration activity of wild-type HICA. Reaction mixtures contained 40 mM bicine (pH 8.50), 1 μM EDTA, and 8.0 mM CO_2 at 25 °C.

binding of a "unique" bicarbonate ion to chains A and C in the protein complex.

Sulfate Ion Binding. Sulfate ion, which is found in the crystallization medium, can be readily identified in electron density maps of HICA-V47A and -G41A. In HICA-V47A in the absence of bicarbonate ion (PDB entry 3E2X), two sulfate ions are bound to a well-recognized anion binding site on the tetramerization interface (*2*), near the side chains of Arg124 of one chain and Arg160, Lys165, and Arg198 of the neighboring chain. In addition, HICA-V47A also binds two sulfate ions in a hydrophobic pocket near the active site near His98, an anion binding mode previously observed for HICA-Y181F (*3*). A fifth sulfate ion is bound on the dimerization interface of HICA-V47A between the Arg64 residues from each chain of the fundamental dimer (Figure 2A). The tetragonal form of HICA-V47A (PDB entry 3E31) does not show clear density for sulfate ion at the tetramerization interface or the hydrophobic pocket near His98. There is some weak electron density on the dimerization interface between adjacent Arg64 residues, but it is not clear if this is attributable to water or a low-occupancy sulfate ion. In PDB entry 3E31, it has been modeled as water.

For HICA-G41A in the absence of bicarbonate ion (PDB entry 3E3G), sulfate ions appear to be bound to the anion binding sites on each of the six tetramerization interfaces. Sulfate ions—four in all, two on special positions—are also observed bound on the dimerization interface between neighboring Arg64 residues (Figure 2B).

Bicarbonate Ion Binding. Two distinct binding modes are observed for bicarbonate ion in both HICA variants V47A and G41A. The first of these is a previously observed noncatalytic (allosteric) binding site near Trp39, Arg64, and Tyr181 (*2*). In HICA-G41A, these include 10 bicarbonate ions bound to chains B (Figure 3A) and D−L. Each of these bicarbonate ions appears to accept hydrogen bonds from Trp39, Arg64, Tyr181, and two water molecules. The carbonyl oxygen of Val47 appears to accept a hydrogen bond from the OH group of bicarbonate (Figure 3A). This hydrogen bonding network has been observed previously for wild-type HICA in a complex with bicarbonate (*2*). In HICA-V47A (PDB entry 3E3F), bicarbonate ions occupy analogous sites in both chains in the asymmetric unit, except that Tyr181 is rotated away and does not appear to interact with the bicarbonate ion in this variant (Figure 3B).

The second binding mode of bicarbonate is in a crevice along the dimerization interface near the neighboring pairs of Arg64 and Glu50 side chains, analogous to the sulfate binding sites shown in Figure 2. In HICA-G41A, only one of the 11 bound bicarbonate ions is bound in this mode, in the interface between chains A and C (Figure 3C), the only two chains of this variant that do not have a bicarbonate ion bound in the previously known noncatalytic bicarbonate binding site near Trp39, Arg64, and Tyr181. In HICA-V47A, the two noncatalytic bicarbonate sites and dimerization interface anion binding site in the asymmetric unit are occupied by bicarbonate ions simultaneously (Figure 3B). The binding of the bicarbonate ion in the dimerization site is the same for both the V47A and G41A variants. The bicarbonate ion appears to accept hydrogen bonds from both Arg64 residues on the dimer interface. One Glu50 side chain appears to accept a hydrogen bond from the OH group of bicarbonate; the other Glu apparently accepts a hydrogen bond from water, which also donates a hydrogen bond to the bicarbonate ion.

We note for the sake of completeness that HICA-V47A (PDB entry 3E3F) harbors a fourth bicarbonate ion bound to the

Table 2: Catalytic Rate Constants for CO_2 Hydration Catalyzed by Wild-Type, G41A, and V47A HICA[a]

	pH 7.50		pH 9.0	
enzyme	k_{cat} (ms^{-1})	k_{cat}/K_m (μM^{-1} s^{-1})	k_{cat} (ms^{-1})	k_{cat}/K_m (μM^{-1} s^{-1})
wild type (*2*)	2.4	0.24	64	5.6
G41A	1.10 ± 0.07	0.42 ± 0.07	5.0 ± 0.3	7.0 ± 1.7
V47A	5.3 ± 0.2	0.88 ± 0.04	140 ± 20	7.0 ± 2.6

[a]Reaction mixtures contained 40 mM 1,2-dimethylimidazole (pH 9.0) or 1-methylimizazole (pH 7.50), 1 μM EDTA, and 250 mM Na_2SO_4 at 25 °C.

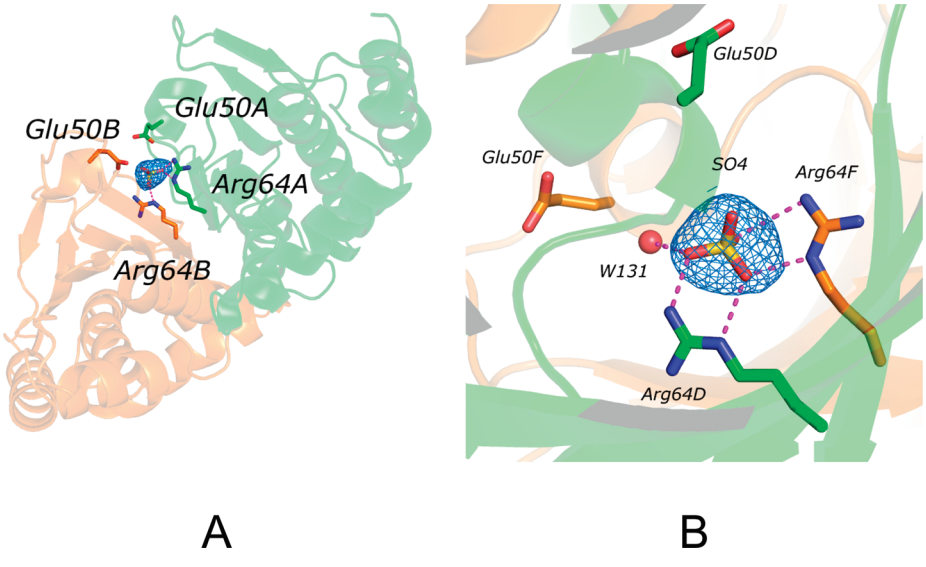

FIGURE 2: Sulfate binding to the dimerization interface of HICA. (A) $F_o - F_c$ omit map of sulfate binding to HICA-V47A, contoured at 3.0σ. The fundamental dimer is colored green (chain A) and orange (chain B). The tetramerization interface is at the bottom right. (B) $F_o - F_c$ omit map of sulfate binding to HICA-G41A, contoured at 2.0σ. Chain D is colored green and chain F orange. This figure was created with Pymol (*21*). In this figure, magenta dashes indicate atoms within hydrogen bonding distance (< 3.5 Å).

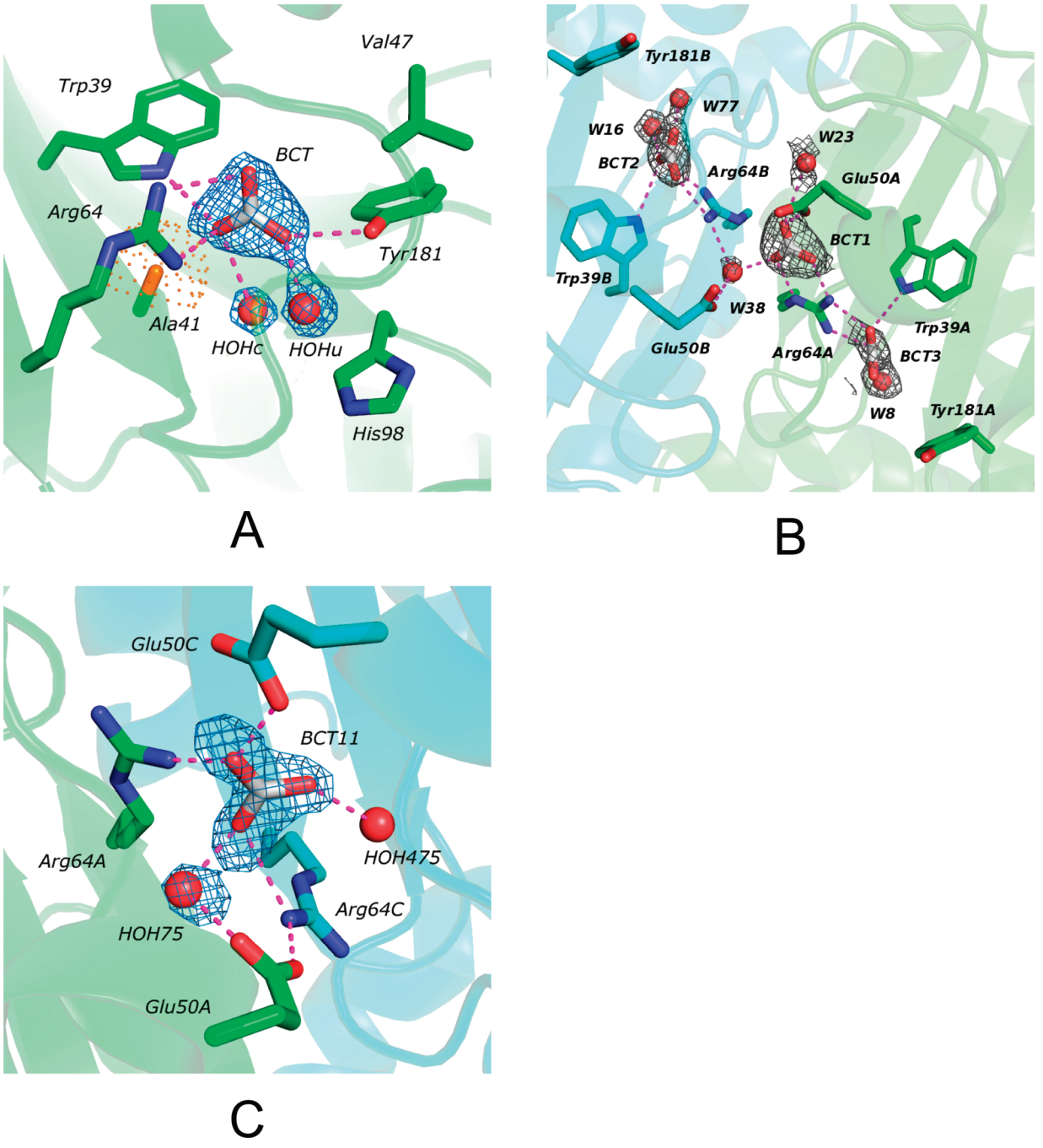

FIGURE 3: Bicarbonate binding to HICA variants. (A) $F_o - F_c$ omit map of bicarbonate binding to the allosteric site of HICA-G41A in chain B, contoured at 3.0σ. HOHc and HOHu represent the "common" and "unique" water molecules in the binding site, respectively (*1*, *2*). The C_β atom of Ala41 is colored orange; orange dots indicate the van der Waals radius of the C_β atom of Ala41. (B) $F_o - F_c$ omit map of bicarbonate binding to the allosteric (BCT2 and BCT3) and escort (BCT1) sites of HICA-V47A, contoured at 1.5σ. Chain A is colored green and chain B cyan. (C) $F_o - F_c$ omit map of bicarbonate binding to the escort site of HICA-G41A, contoured at 3.0σ. Chain A is colored green and chain C cyan. This figure was created with Pymol (*21*). In this figure, magenta dashes indicate atoms within hydrogen bonding distance (<3.5 Å).

tetramerization interface where anions such as sulfate (*2*) or phosphate (*3*) have been previously observed to bind.

DISCUSSION

HICA variants V47A and G41A were expressly constructed to critically test the effect of steric crowding in the noncatalytic, allosteric bicarbonate binding site of HICA. One might have expected HICA-V47A to have lost the steric coupling mechanism required to expel bicarbonate ion from the T state and stabilize the R state, leading to an enzyme with reduced activity, yet HICA-V47A has k_{cat} and k_{cat}/K_m values for CO_2 hydration that are comparable to those of the wild-type enzyme and still shows a dramatic decrease in k_{cat} and k_{cat}/K_m at pH < 8.0 that is typical of type II β-CAs (*1*). One might expect that HICA-G41A would be incapable of binding allosteric bicarbonate because of the steric interference of the methyl side chain of Ala41 in this variant, leading to an enzyme with enhanced activity, especially at low pH where the inactive T state is thought to predominate (*2*, *3*); however, HICA-G41A has k_{cat}/K_m values for CO_2 hydration similar to those of the wild-type enzyme, and its k_{cat} at high pH is actually significantly lower than the wild-type value. Why

mutation of Gly41 would have such a significant effect on k_{cat} is not obvious from either a mechanistic or structural viewpoint. In addition, it is clear from the crystallographic data (Figure 3A) that bicarbonate ion can still bind in the noncatalytic, allosteric site. Apparently, the β-sheet containing the variant Ala41 residue and/or the bicarbonate ion has subtly shifted sufficiently to be able to accommodate both the methyl side chain of Ala41 and bicarbonate ion in the allosteric binding site, so it would appear that the catalytic activity of the enzyme and the function of the allosteric bicarbonate binding site are not so easily disrupted by single side chain alterations at Val47 or Gly41.

Evidence for a Bicarbonate "Escort" Site. Unexpectedly, HICA variants V47A and G41A in the presence of bicarbonate ion have revealed a highly probable intermediate bicarbonate binding site on the dimerization interface of the enzyme near a pair of Arg64 and Glu50 residues (Figures 3B,C). Bicarbonate binding to this site has been observed previously for allosteric site variant Y181F (*3*), as well as here for one of the dimerization interfaces of 12 protein chains in the asymmetric unit of variant G41A (Figure 3C), and for variant V47A (Figure 3B). The observation of this bicarbonate binding site in multiple crystal structures suggests that it is not artifactual and may be functionally relevant. The location of this bicarbonate binding in the proximity of the allosteric bicarbonate binding site strongly suggests that it represents an intermediate along the ingress and egress route for allosteric bicarbonate. We propose designating this bicarbonate binding site the escort site, a jumping-off point for bicarbonate ions transitioning between bulk solution and the allosteric binding site of HICA. Because the structures of the wild-type enzyme and the variants described here are identical overall and in the escort site region, it seems likely that bicarbonate ions can bind to this site in the wild-type enzyme as well, although anion binding to the escort site region in the wild-type enzyme has not been observed crystallographically (*2*). The crystal structure of HICA-V47A in a complex with bicarbonate ion suggests that the allosteric and escort binding sites are not mutually exclusive but can be occupied simultaneously (Figure 3B). It seems remarkable that it is possible to "catch" the binding of bicarbonate ion in the escort site but not the allosteric site in HICA-Y181F (*3*) and chains A and C only for HICA-G41A (Figure 3C), while both the escort and allosteric sites are both occupied in HICA-V47A (Figure 3B). One can only assume that variations in intermolecular contacts and solvent channels in the various crystal forms and variants of HICA are responsible for the lucky happenstance of observing bicarbonate binding at the escort site.

Examination of the HICA-V47A structure (PDB entry 3E3F) with CAVER (*16*, *17*) reveals plausible entry and exit routes for allosteric bicarbonate ion (Figure 4). One of these routes (colored orange) passes down the dimerization interface, past opposing Glu50 and Arg64 residues in this crevice and into the allosteric site. Another route (colored pink) enters and exits just to the side of the dimerization interface, among Arg46, Ala47, and Leu52. This route appears to be possible in HICA-V47A only because Tyr181 has rotated away from the allosteric site and is not engaged in a hydrogen bonding interaction with allosteric bicarbonate ion. In wild-type HICA (*2*) and the G41A variant (Figure 3A), Tyr181 is engaged in a hydrogen bonding interaction with both the allosteric bicarbonate ion and the main chain amide nitrogen of Val47 and/or the unique water (*1*, *2*). At first glance, the intermolecular contacts in the bicarbonate escort site look odd. While it is certainly chemically reasonable to expect

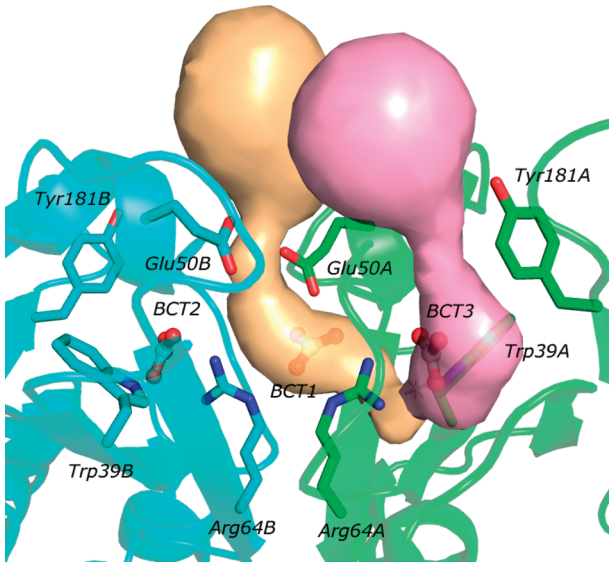

FIGURE 4: Depiction of tunnels leading to the allosteric bicarbonate binding site in chain A of HICA-V47A (PDB entry 3E3F). Key residues in the allosteric and escort sites are depicted as sticks. Chain A is colored green and chain B cyan. Bicarbonate ions BCT2 and BCT3 are bound to the allosteric sites; BCT1 is bound to the escort site. Tunnels are depicted as colored surfaces leading to the BCT3 allosteric site. The orange-colored tunnel passes through the escort site. The pink-colored tunnel passes by Tyr181, which is rotated away from the allosteric site in this HICA variant. This figure was created with Pymol (*21*). Tunnels were computed using CAVER 2.0 (*16*, *17*).

that bicarbonate ion would interact with the pair of Arg64 residues in this site, the presumably negatively charged pair of Glu50 residues looks less inviting because of the potential charge repulsion involved. Nevertheless, the data suggest that one Glu residue, Glu50A in HICA-V47A (Figure 3B) and Glu50C in HICA-G41A (Figure 3C), is within direct hydrogen bonding distance of one of the bicarbonate oxygen atoms, presumably the oxygen of the OH group. The other Glu residue, Glu50B in HICA-V47A (Figure 3B) and Glu50A in HICA-G41A (Figure 3C), appears to interact with bicarbonate ion through a water molecule which likely donates hydrogen bonds to both Glu50 and bicarbonate ion.

Precedent for the interaction of carboxylates with protein-bound bicarbonate ion comes from unlikely sources: cyclopropane fatty acid synthase from *E. coli* (*18*) and the mycolic acid cyclopropane synthases from *Mycobacterium tuberculosis* (*19*), in which bicarbonate ion is thought to be a catalytically essential cofactor. In these synthases, the bound bicarbonate ion interacts with three hydrogen bond donors: a Tyr, a His, and a backbone amide. A single Glu side chain interacts directly with the bicarbonate ion presumably as a hydrogen bond acceptor (Figure S1 of the Supporting Information). This is analogous to HICA, in which two Arg residues and one water molecule act as hydrogen bond donors, and the Glu side chain acts as a hydrogen bond acceptor with bicarbonate ion. Although Courtois and Ploux (*18*) speculated that the His residue of *E. coli* cyclopropane fatty acid synthase was neutral, it seems more likely that this residue is protonated to help neutralize negative charge in the binding site, analogous to the Arg residues in HICA.

Activation of HICA by Sulfate Ion. The existence of a bicarbonate escort site in HICA offers a possible explanation for the observed activation of HICA by sulfate ion in vitro. This phenomenon has been well-known since the initial kinetic studies

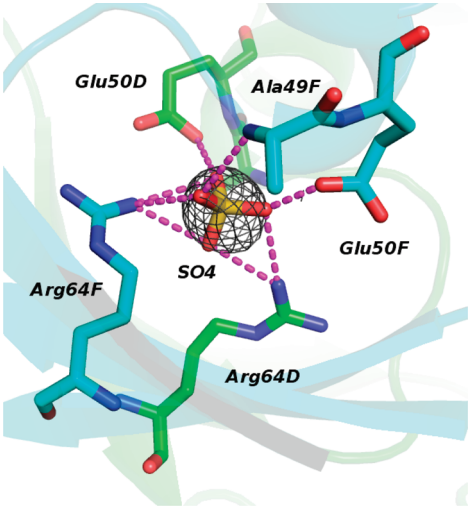

FIGURE 5: $F_o - F_c$ omit map of sulfate binding to the escort site in HICA-Y181F (PDB entry 3E28) (*3*), contoured at 2.0σ. Chain D is colored green and chain F cyan. This figure was created with Pymol (*21*). Magenta dashes indicate atoms within hydrogen bonding distance (<3.5 Å).

of HICA (*2*) but has never had a satisfactory explanation. A number of X-ray crystallographic structures of HICA and its variants, including Y181F [PDB entry 3E28 (Figure 5)] (*3*) and variants G41A (Figure 3B) and V47A (Figure 3A), bind sulfate ion at the bicarbonate escort site in the absence of bicarbonate ion. Thus, it seems likely that sulfate ion acts as a competitive inhibitor for bicarbonate ion at the escort site, hindering access of bicarbonate ion to produce the inactive, T state of the enzyme. In the absence of sulfate ion in vitro, very little or no CO_2 hydration activity can be observed for HICA, most likely due to the accumulation of the product, HCO_3^-, which quickly converts the enzyme to the T state. The presence of sulfate ion at the escort site would prevent the ingress of bicarbonate ion to the allosteric site, largely preserving enzyme activity during the data collection period for CO_2 hydration, which is typically 100−1000 ms for stopped-flow spectrophotometry. One might reasonably expect non-Michaelis−Menten kinetics in such a complex system in which sulfate and product (bicarbonate) are competing for the escort site. However, no significant deviation from apparent Michaelis−Menten kinetics was observed for either the wild-type enzyme or variant G41A or V47A during the time span of the stopped-flow measurements. A possible explanation is that the reorganization of the enzyme from the active, R state to the inactive, T state is very likely to require a time scale significantly longer than that required for stopped-flow kinetics, perhaps in the seconds to tens of seconds.

It does not seem likely that the binding of sulfate to HICA is physiologically relevant, as the sulfate concentrations required for the maximal effect (200−400 mM) are much higher than intracellular concentrations of sulfate ion. However, it is possible that other anions could also bind to the escort site. HICA variant W39F, which was crystallized from low concentrations (40−80 mM) of ammonium phosphate (PDB entry 3E24), was found to have phosphate ion bound to the bicarbonate escort site (*3*). It is tempting to speculate that physiological concentrations (millimolar) of phosphate ion could act as an indirect allosteric effector of HICA by hindering the ability of bicarbonate ion to shift the allosteric equilibrium of HICA toward the T state in vivo.

CONCLUSION

HICA variants V47A and G41A are similar to wild-type HICA in overall structure and catalytic ability toward CO_2 hydration. Despite these variants having significantly different sterics in the allosteric binding site for bicarbonate compared to HICA, crystals of these protein variants prepared in the presence of bicarbonate ion are found to have bicarbonate present in the allosteric site. In addition, these variants exhibit an additional bicarbonate binding site on the dimerization interface, a bicarbonate escort site, that is likely to be an intermediate binding site along the ingress and egress route for allosteric bicarbonate. The kinetic and structural evidence reported here suggests that sulfate, and perhaps other anions, can bind to the escort site and prevent the binding of bicarbonate ion to the allosteric site, thereby "activating" the enzyme by stabilizing the active R state relative to the inactive T state of the enzyme.

ACKNOWLEDGMENT

Research was conducted at the Cornell High Energy Synchrotron Source (CHESS), which is supported by the National Science Foundation (NSF) and the National Institutes of Health/National Institute of General Medical Sciences, under NSF Grant DMR-0225180, using the Macromolecular Diffraction at CHESS (MacCHESS) facility, which is supported by Grant RR-01646 from the National Institutes of Health, through its National Center for Research Resources.

SUPPORTING INFORMATION AVAILABLE

Bicarbonate binding site in *M. tuberculosis* mycolic acid cyclopropane synthase CmaA2, which shares key features with the bicarbonate escort site in HICA (Figure S1). This material is available free of charge via the Internet at http://pubs.acs.org.

REFERENCES

1. Rowlett, R. S. (2010) Structure and catalytic mechanism of the β-carbonic anhydrases. *Biochim. Biophys. Acta 1804*, 362–373.
2. Cronk, J. D., Rowlett, R. S., Zhang, K. Y. J., Tu, C., Endrizzi, J. A., Lee, J., Gareiss, P. C., and Preiss, J. R. (2006) Identification of a Novel Noncatalytic Bicarbonate Binding Site in Eubacterial β-Carbonic Anhydrase. *Biochemistry 45*, 4351–4361.
3. Rowlett, R. S., Tu, C., Lee, J., Herman, A. G., Chapnick, D. A., Shah, S. H., and Gareiss, P. C. (2009) Allosteric Site Variants of *Haemophilus influenzae* β-Carbonic Anhydrase. *Biochemistry 48*, 6146–6156.
4. Sarkar, G., and Sommer, S. S. (1990) The Megaprimer Method of Site-Directed Mutagenesis. *BioTechniques 8*, 404–407.
5. Khalifah, R. G. (1971) Carbon dioxide hydration activity of carbonic anhydrase. I. Stop-flow kinetic studies on the native human isoenzymes B and C. *J. Biol. Chem. 246*, 2561–2573.
6. Pocker, Y., and Bjorkquist, D. W. (1977) Comparative studies of bovine carbonic anhydrase in water and water-d2. Stopped-flow studies of the kinetics of interconversion of carbon dioxide and bicarbonate(1−) ion. *Biochemistry 16*, 5698–5707.
7. Ghannam, A. F., Tsen, W., and Rowlett, R. S. (1986) Activation parameters for the carbonic anhydrase II-catalyzed hydration of carbon dioxide. *J. Biol. Chem. 261*, 1164–1169.
8. Rowlett, R. S., Gargiulo, N. J., III, Santoli, F. A., Jackson, J. M., and Corbett, A. H. (1991) Activation and inhibition of bovine carbonic anhydrase III by dianions. *J. Biol. Chem. 266*, 933–941.
9. Leslie, A. G. W. (1992) Recent changes to the MOSFLM package for processing film and image data, Joint CCP4 and ESF-EACMB Newsletter on Protein Crystallography.
10. Collaborative Computational Project, Number 4 (1994) The CCP4 Suite: Programs for protein crystallography. *Acta Crystallogr. D50*, 760–763.
11. McCoy, A. J., Grosse-Kunstleve, R. W., Adams, P. D., Winn, M. D., Storoni, L. C., and Read, R. J. (2007) Phaser crystallographic software. *J. Appl. Crystallogr. 40*, 658–674.

12. Murshudov, G. N., Vagin, A. A., and Dodson, E. J. (1997) Refinement of macromolecular structures by the maximum-likelihood method. *Acta Crystallogr. D53*, 240–255.
13. Emsley, P., and Cowtan, K. (2004) Coot: Model-building tools for molecular graphics. *Acta Crystallogr. D60*, 2126–2132.
14. Winn, M. D., Isupov, M. N., and Murshudov, G. N. (2001) Use of TLS parameters to model anisotropic displacements in macromolecular refinement. *Acta Crystallogr. D57*, 122–133.
15. Innocenti, A., Vullo, D., Scozzafava, A., and Supuran, C. T. (2005) Carbonic anhydrase inhibitors. Inhibition of isozymes I, II, IV, V, and IX with anions isosteric and isoelectronic with sulfate, nitrate, and carbonate. *Bioorg. Med. Chem. Lett. 15*, 567–571.
16. Petrek, M., Otyepka, M., Banas, P., Kosinova, P., Koca, J., and Damborsky, J. (2006) CAVER: A new tool to explore routes from protein clefts, pockets and cavities. *BMC Bioinf. 7*, 316.
17. Damborsky, J., Petrek, M., Banas, P., and Otyepka, M. (2007) Identification of tunnels in proteins, nucleic acids, inorganic materials and molecular ensembles. *Biotechnol. J. 2*, 62–67.
18. Courtois, F., and Ploux, O. (2005) *Escherichia coli* cyclopropane fatty acid synthase: Is a bound bicarbonate ion the active-site base? *Biochemistry 44*, 13583–13590.
19. Huang, C. C., Smith, C. V., Glickman, M. S., Jacobs, W. R., and Sacchettini, J. C. (2002) Crystal structures of mycolic acid cyclopropane synthases from *Mycobacterium tuberculosis*. *J. Biol. Chem. 277*, 11559–11569.
20. Engh, R. A., and Huber, R. (1991) Accurate bond and angle parameters for X-ray protein structure refinement. *Acta Crystallogr. A47*, 392–400.
21. DeLano, W. L. (2002) The PyMOL Molecular Graphics System, DeLano Scientific, San Carlos, CA.